Geochemical Constraints on the Origin of the Ni–Cu Sulfide Ores in the Tejadillas Prospect (Cortegana Igneous Complex, SW Spain)

Rubén Piña,[1] Fernando Gervilla,[2] Lorena Ortega[1] and Rosario Lunar[1]

[1]*Departamento de Cristalografía y Mineralogía, Facultad de Ciencias Geológicas, Universidad Complutense de Madrid, c/ José Antonio Novais s/n, Madrid, Spain, and* [2]*Departamento de Mineralogía y Petrología and Instituto Andaluz de Ciencias de la Tierra, Facultad de Ciencias, Universidad de Granada-CSIC, Avda. Fuentenueva s/n, Granada, Spain*

Abstract

After the discovery of the Aguablanca ore deposit (the unique Ni–Cu mine operating in SW Europe), a number of mafic-ultramafic intrusions bearing Ni–Cu magmatic sulfides have been found in the Ossa–Morena Zone of the Iberian Massif (SW Iberian Peninsula). The Tejadillas prospect is one of these intrusions, situated close to the border between the Ossa–Morena Zone and the South Portuguese Zone of the Iberian Massif. This prospect contains an average grade of 0.16 wt % Ni and 0.08 wt % Cu with peaks of 1.2 wt % Ni and 0.2 wt % Cu. It forms part of the Cortegana Igneous Complex, a group of small mafic-ultramafic igneous bodies located 65 km west of the Aguablanca deposit. In spite of good initial results, exploration work has revealed that sulfide mineralization is much less abundant than in Aguablanca. A comparative study using whole-rock geochemical data between Aguablanca and Tejadillas shows that the Tejadillas igneous rocks present a lower degree of crustal contamination than those of Aguablanca. The low crustal contamination of the Tejadillas magmas inhibited the assimilation of significant amounts of crustal sulfur to the silicate magmas, resulting in the sparse formation of sulfides. In addition, Tejadillas sulfides are strongly depleted in PGE, with total PGE contents ranging from 14 to 81 ppb, the sum of Pd and Pt, since Os, Ir, Ru and Rh are usually below or close to the detection limit (2 ppb). High Cu/Pd ratios (9700–146,000) and depleted mantle-normalized PGE patterns suggest that the Tejadillas sulfides formed from PGE-depleted silicate magmas. Modeling has led us to establish that these sulfides segregated under R-factors between 1000 and 10,000 from a silicate melt that previously experienced 0.015% of sulfide extraction. All these results highlight the importance of contamination processes with S-rich crustal rocks and multiple episodes of sulfide segregations in the genesis of high-tenor Ni–Cu–PGE ore deposits in mafic-ultramafic intrusions of the region.

1. Introduction

Crustal contamination, fractional crystallization and magma mixing are common mechanisms that trigger sulfur saturation in mantle-derived magmas (*i.e.*, Barnes & Lightfoot, 2005). Among these processes, crustal contamination is responsible for the formation of a number of Ni–Cu sulfide deposits via assimilation

of either crustal sulfur (e.g., Voisey's Bay, Canada, Ripley *et al*., 1999; Noril'sk, Russia, Lightfoot & Keays, 2005; Kabanga, Tanzania, Maier *et al*., 2010) or SiO_2-rich materials (e.g., Nebo-Babel, Australia, Seat *et al*., 2009; Baimazhai & Kalatongke, China, Wang *et al*., 2006; Zhang *et al*., 2009). Assimilation of S-rich crustal materials causes an increase of the sulfur content in the contaminated magma that may exceed its sulfur capacity resulting in sulfide over saturation (Wendlandt, 1982). Similarly, addition of SiO_2 to the system through the assimilation of siliceous materials decreases the sulfur solubility in mafic magmas and thus may also trigger sulfur saturation (Li & Naldrett, 1993).

In the Aguablanca Ni–Cu ore deposit (the closest Ni–Cu operating mine to the Cortegana Igneous Complex), the assimilation of pyrite-rich black slate of the Late Neoproterozoic Serie Negra Formation by silicate melts was the key factor for the sulfur saturation and subsequent sulfide segregation (Casquet *et al*., 2001; Tornos *et al*., 2001; Piña *et al*., 2010). As a consequence, exploration efforts focused on the identification of mafic-ultramafic bodies in the region intruding the Serie Negra Formation and showing evidence of crustal contamination, and a number of small Ni–Cu sulfide-bearing mafic-ultramafic igneous bodies, such as Argallón, Brovales and Cortegana, were identified (Martín-Izard *et al*., 2006; Tornos *et al*., 2006).

The Cortegana Igneous Complex contains significant amounts of base-metal sulfides (drill holes intercepted mineralized zones with up to 1.36 wt. % Ni and 0.2 wt. % Cu). However, in spite of good initial results, detailed exploration work has shown that the sulfide mineralization at Cortegana is much less abundant than in Aguablanca. Preliminary studies also show that sulfide-mineralized igneous rocks in Cortegana exhibit less evidence of crustal contamination than those of Aguablanca (Tornos *et al*., 2006; Piña *et al*., 2009). Whether the low degree of contamination was the key factor for the scarce segregation of sulfides in Cortegana is still unknown. Thus, the study of the Cortegana Igneous Complex and its comparison with the Aguablanca deposit provide an excellent opportunity to evaluate the role played by crustal contamination in the formation of sulfide ores in mafic-ultramafic intrusions of the region.

The Cortegana Igneous Complex comprises a number of small intrusive bodies named Tejadillas, Sojalva, El Merendero, La Caballona and Tabarca. The sulfide mineralization is located in the Tejadillas igneous body, the largest prospect in where exploration work has mostly focused. In this contribution, we present detailed mineralogical and geochemical results of the Tejadillas prospect, reporting mineral compositions and whole rock concentrations of major and trace elements, including platinum-group elements (PGE). In addition to examining the effect caused by crustal contamination on the genesis of the sulfides, we use these results to address some questions related to: (i) nature of parental magmas of the intrusion; (ii) controls on the sulfide compositions; and (iii) model of sulfide genesis in the Tejadillas prospect of the Cortegana Igneous Complex with implications for regional exploration of Ni–Cu deposits in SW Spain.

2. Geological background

The Cortegana Igneous Complex is located within the Ossa–Morena Zone of the Iberian Massif, close to the border with the South Portuguese Zone (Fig. 1a). These zones constitute the southernmost tectonic domains of the Iberian Massif, which includes extensive outcrops of pre-Mesozoic rocks in the Iberian Peninsule (Quesada, 1991). The complex occurs in the Aracena Metamorphic Belt, a WNW-ESE-oriented, few km wide and more than 100 km long band (Fig. 1) composed of high-T/low-P metamorphic rocks (mostly gneisses, marbles, calc-silicate rocks and amphibolites) (Castro *et al*., 1996; Díaz Azpiroz *et al*., 2004). The metamorphic event took place during the Variscan orogeny ($^{40}Ar/^{39}Ar$ ages range from 343 to 328 Ma, Dallmeyer *et al*., 1993; Castro *et al*., 1999), affecting volcanic and sedimentary rocks of Late Proterozoic to Cambrian age. The metamorphism developed mostly under amphibolite to granulite facies (Patiño Douce *et al*., 1997; Díaz Azpiroz *et al*., 2004), reaching eclogite facies up to 650°C and 14–16 kbar in the Beja-Acebuches amphibolites (Fonseca *et al*., 1999). The Aracena Metamorphic Belt has been divided in two lithological domains (Fig. 1b) (Castro *et al*., 1996): southern oceanic domain (Beja-Acebuches amphibolites) and northern continental domain. The Beja-Acebuches amphibolites are regarded to be metamorphosed oceanic crust with MORB-type affinities (Quesada *et al*., 1994; Castro *et al*., 1996). The continental domain is made up by high-, medium- and low-grade metamorphic rocks with increasing metamorphic grade from north toward south. The Cortegana Igneous Complex intrudes in the high-grade, southern part of the continental domain (Fig. 1b), where metamorphic rocks consist of pelitic gneisses, calc-silicate rocks, marbles and amphibolites of Late Neoproterozoic to Early Cambrian age.

The Cortegana Igneous Complex comprises a number of small intrusive bodies (Tejadillas, Sojalva,

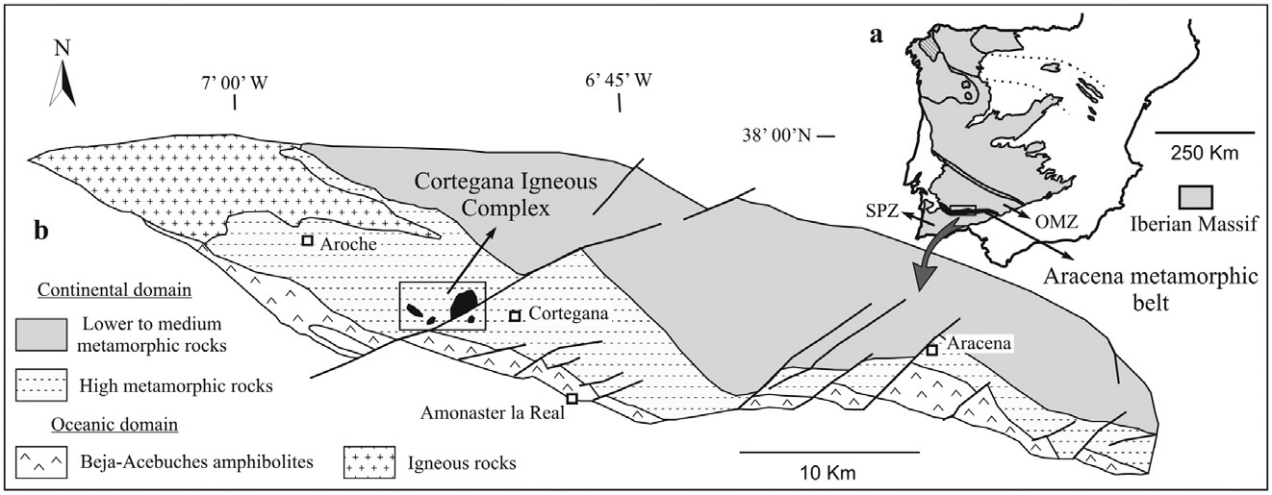

Fig. 1 (a) Location of the Aracena Metamorphic Belt between the Ossa–Morena (OMZ) and South-Portuguese (SPZ) Zones of the Iberian Massif. (b) Simplified geologic map of the Aracena Metamorphic Belt showing the location of the Cortegana Igneous Complex. Modified from De la Rosa *et al*. (2002).

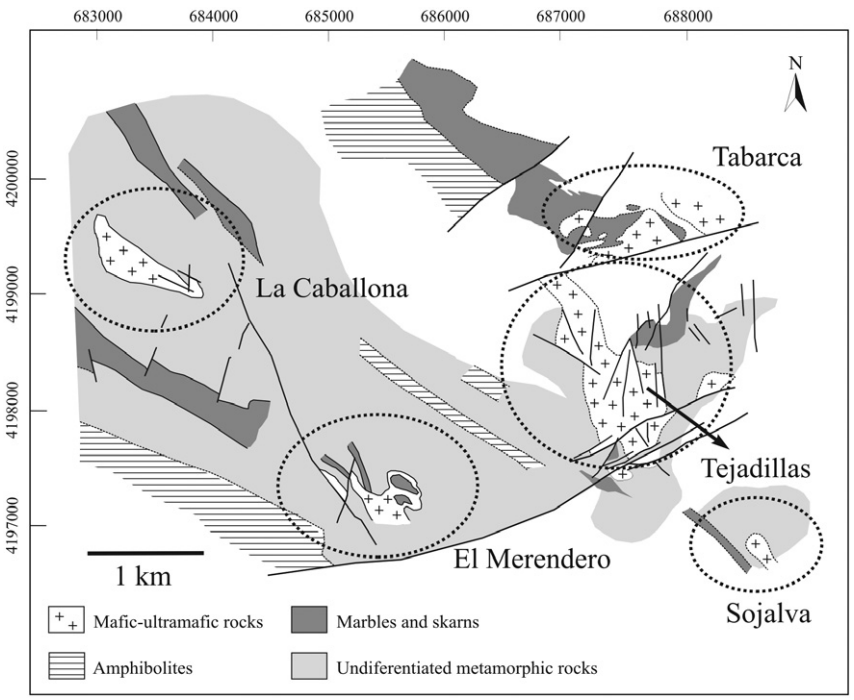

Fig. 2 Schematic geologic map, showing the different intrusive bodies that constitute the Cortegana Igneous Complex (La Caballona, El Merendero, Tabarca, Tejadillas and Sojalva).

El Merendero, La Caballona and Tabarca, Fig. 2) commonly mapped as diorites and quartz-diorites. Several cores drilled by Lundin Mining (the owner of the exploration rights of the prospects) revealed that the Cortegana Igneous Complex is made up of mafic-ultramafic cumulates consisting of peridotite (mostly hornblende-bearing harzburgite), gabbronorite, gabbro, norite and, locally, quartz-diorite. The most primitive rocks, i.e., peridotites and gabbronorites, host variable amounts of disseminated and minor semi-massive Fe-Ni–Cu sulfides. Radiometric dating gave an age of 336.2 ± 1.7 Ma for the Cortegana Igneous Complex ($^{40}Ar/^{39}Ar$ method on phlogopite, Tornos *et al*., 2006), similar to the age estimated for the

Aguablanca intrusion (341 ± 1.5 Ma, U/Pb method on zircons, Romeo *et al*., 2006). Among the intrusive bodies of the Cortegana Igneous Complex, Tejadillas is the most mineralized, locally hosting sulfide-rich zones with relatively high metal grades (up to 1.4 wt. % Ni and 0.2 wt. % Cu). The Tejadillas prospect consists of a poorly exposed, tabular-shaped body of roughly 1.4 km long and 0.7 km wide (Fig. 2). Its long axis strikes north-northwest. Overall, the intrusion is more mafic in its inner zone than at the margins, where it becomes more leucocratic.

3. Analytical methods

A total of 33 rock samples were collected from two cores (TJ-5 and TJ-17) drilled in the Tejadillas intrusive body by Lundin Mining. These samples represent the different lithological types present in the prospect and include variably mineralized rocks. Polished thin sections were prepared and studied by transmitted and reflected light optical microscope. Silicate and sulfide compositions were determined by wavelength-dispersive X-ray analyses using a JEOL Superprobe JXA 8900 M in the Centro de Microscopía Electrónica of the University Complutense of Madrid. The analytical conditions were: accelerating voltage of 15 kV, beam current of 20 nA and beam diameter of 4 μm. Counting times ranged from 20 to 60 s. Representative analyses of primary silicates, including olivine, pyroxene, plagioclase and amphibole, and sulfides are summarized in Tables 1 and 2, respectively.

Twenty-one representative rock samples of the Tejadillas prospect were analyzed for whole rock geochemistry in Genalysis Laboratory Services Pty. Ltd, Maddington (Western Australia). Major oxides, S, Ni, Cu and Cr contents were determined by X-ray fluorescence spectrometry (XRF) on fused beads. Platinum-group elements (PGE) and Au were analyzed by inductively coupled plasma-mass spectrometer (ICP-MS) after nickel sulfide fire assay collection. Detection limits for noble metals were 5 ppb for Au, 2 ppb for Ir, Os, Ru, Pd and Pt and 1 ppb for Rh. All remaining trace elements (including REE) were analyzed by ICP-MS after multi-acid digestion.

4. Petrographical descriptions and mineral chemistry

The Tejadillas mafic-ultramafic prospect is made up by medium to coarse-grained igneous cumulates including hornblende-bearing harzburgite, olivine gabbronorite, norite, gabbronorite, gabbro *s.s.* (*sensu strictu*, mostly plagioclase + clinopyroxene) and quartz-diorite. In general, the intrusion is dominated by norite and gabbronorite. The primary mineralogy and cumulate textures are often obscured by the intense pervasive alteration characterized by variable replacement of olivine by serpentine, pyroxene by amphibole and chlorite, and plagioclase by sericite, zoisite and chlorite. The boundaries between the different rock types are gradational and are controlled by variations in the modal contents in olivine, pyroxene and plagioclase. The contact with the country host rocks is marked by the presence of orbicular-textured rocks consistent in gabbros *s.s.* with rounded to angular xenoliths of country metamorphic rocks (mainly, calc-silicate hornfels). These xenoliths show well-marked boundaries with evidence of poor digestion by the host magmas.

The ultramafic rocks are characterized by relatively high contents of primary amphibole. These rocks are mainly hornblende-bearing harzburgites. They consist of meso- to orthocumulates formed by cumulus olivine ($Fo_{79–83}$) and orthopyroxene (Mg# = 0.81–0.83) with intercumulus plagioclase ($An_{88–96}$), amphibole (pargasite hornblende and tschermakiite) and minor phlogopite. Olivine occurs as rounded to subrounded grains commonly enclosed, totally or partially, by poikilitic amphibole (Fig. 3a). Textural relationships suggest that olivine started to crystallize before orthopyroxene. More differentiated ultramafic rocks also contain minor cumulus clinopyroxene (Mg# = 0.84–0.88) and, locally, abundant plagioclase. Nickel contents in olivine and pyroxene are very low, below 0.20 wt % and 0.07 wt %, respectively.

With increasing pyroxene contents, olivine decreases and the hornblende-bearing harzburgite grades progressively into hornblende-bearing olivine gabbronorite. In this rock, cumulus pyroxene predominates over olivine, which often occurs enclosed by clinopyroxene oikocrysts and poikilitic amphibole (pargasite hornblende). Orthopyroxene occurs as idiomorphic cumulus crystals with heterogeneous grain size, and plagioclase is typically intercumulus (Fig. 3b). In these rocks, olivine ($Fo_{75–78}$) and orthopyroxene (Mg# = 0.79–0.80) are slightly richer in Fe than in harzburgite. The forsterite content of olivine in harzburgite and olivine gabbronorite is positively correlated with the Mg# values of orthopyroxene (ρ = 0.88, not shown), suggesting a fractional crystallization trend. Mg# values of clinopyroxene range from 0.85 to 0.87 and plagioclase is rich in Ca ($An_{88–90}$).

Table 1 Representative electron microprobe analyses of olivine, pyroxene, plagioclase and amphibole of igneous rocks from Tejadillas prospect, Cortegana Igneous Complex

Phase	Ol	Ol	Ol	Opx	Opx	Opx	Opx	Cpx	Cpx	Cpx	Cpx	Plag	Plag	Plag	Plag	Plag	Plag	Amp	Amp	Amp
Rock type	Hz	Hz	Hz	Hz	Ol Gn	Gn	Q-d	Hz	Ol Gn	N	G	Hz	Ol Gn	N	GN	G	Q-d	Hz	GN	Q-d
wt. % oxide																				
SiO_2	38.69	39.14	38.36	55.35	54.12	54.80	55.07	51.97	53.27	52.83	53.42	43.69	45.48	47.71	46.03	46.87	58.04	44.39	49.81	53.30
TiO_2	<	<	<	0.02	0.14	0.08	0.11	0.43	0.04	0.28	0.12	<	<	<	<	<	<	1.66	0.83	0.60
Al_2O_3	0.01	<	<	1.39	1.51	0.79	0.57	2.96	0.65	1.51	0.72	36.64	34.48	33.83	34.70	33.58	25.68	13.12	7.02	2.85
Cr_2O_3	0.09	<	<	0.11	0.05	0.10	0.11	0.28	0.10	0.13	0.06	n.a.	n.a.	n.a.	n.a.	n.a.	n.a.	0.36	0.29	0.22
FeO	18.53	17.52	21.78	11.41	13.26	13.37	14.58	4.64	4.27	5.38	5.04	0.13	0.08	0.07	0.08	0.12	0.01	5.93	5.71	5.80
MnO	0.26	0.19	0.03	0.22	0.03	0.39	0.07	0.13	0.04	0.25	0.15	<	<	<	<	<	<	0.08	0.13	0.02
MgO	41.88	44.00	40.11	30.50	28.46	29.26	28.39	15.99	15.92	16.09	15.50	<	<	<	<	<	<	16.47	18.95	20.67
CaO	0.02	<	0.01	0.60	1.13	0.46	0.71	24.18	24.81	22.76	24.43	19.81	18.63	16.49	17.42	16.93	7.89	12.43	11.73	12.33
Na_2O	0.02	<	0.02	0.02	0.02	0.01	0.01	0.09	0.11	0.24	0.10	0.48	1.15	2.32	1.66	1.90	7.17	1.71	1.09	0.51
K_2O	<	<	0.01	<	<	<	<	<	<	<	0.01	<	<	0.02	0.02	0.04	0.28	0.54	0.46	0.16
NiO	0.04	0.11	0.08	0.04	<	0.05	<	<	<	0.01	0.04	n.a.	n.a.	n.a.	n.a.	n.a.	n.a.	<	<	0.02
Total	99.54	100.96	100.40	99.66	98.72	99.31	99.62	100.67	99.21	99.48	99.59	100.75	99.82	100.44	99.91	99.44	99.07	96.69	96.02	96.48
apfu																				
Si	0.994	0.986	0.991	1.959	1.954	1.965	1.980	1.891	1.968	1.948	1.974	2.010	2.102	2.178	2.119	2.164	2.622	6.361	7.087	7.493
Al				0.058	0.064	0.034	0.024	0.127	0.028	0.066	0.031	1.986	1.879	1.820	1.883	1.823	1.367	2.218	1.176	0.472
Ti					0.004	0.002	0.003	0.012	0.001	0.008	0.003							0.179	0.089	0.063
Fe^{3+}				0.021	0.021	0.030	0.007	0.066	0.039	0.036	0.021							0.183	0.280	0.377
Fe^{2+}	0.398	0.369	0.471	0.318	0.380	0.372	0.432	0.077	0.094	0.131	0.135							0.528	0.399	0.066
Mg	1.604	1.652	1.544	1.609	1.531	1.564	1.522	0.867	0.877	0.884	0.854							3.522	4.020	4.331
Mn	0.006	0.004	0.001	0.007	0.001	0.012	0.002	0.004	0.001	0.008	0.005							0.009	0.016	0.002
Cr	0.002			0.003	0.001	0.003	0.003	0.008	0.003	0.004	0.002							0.041	0.033	0.025
Ni	0.001	0.002	0.002	0.001		0.001					0.001									
Ca	0.001			0.023	0.044	0.018	0.027	0.943	0.982	0.899	0.967	0.976	0.922	0.807	0.859	0.838	0.381	1.910	1.787	1.856
K											0.001			0.001	0.001	0.002	0.628	0.098	0.084	0.029
Na	0.001		0.001	0.001	0.001	0.001		0.006	0.008	0.017	0.007	0.043	0.103	0.206	0.148	0.170	0.016	0.475	0.302	0.139
Total	3.007	3.013	3.010	4.000	4.001	4.002	4.000	4.001	4.001	4.001	4.001	5.015	5.006	5.012	5.010	4.997	5.014	15.524	15.273	14.853
Mg#	0.80	0.82	0.77	0.83	0.79	0.80	0.78	0.86	0.87	0.84	0.85							0.83	0.86	0.91
%An												95.8	90.0	79.6	85.2	83.0	37.2			

Ol = olivine; Opx = orthopyroxene; Cpx = clinopyroxene; Plag = plagioclase; Amp = amphibole. Hz = hornblende-bearing harzburgite; Ol Gn = olivine-bearing gabbronorite; Gn = gabbronorite; N = norite; Q-d = quartz-diorite. All Fe as FeO. apfu: atoms per formula unit. Atomic concentrations recalculated to 4, 6, 8 and 23 oxygens for olivine, pyroxene, plagioclase and amphibole, respectively. Mg# = (Mg/Mg+Fetot), An = (Ca/Ca+Na). Mg# and An calculated from atomic concentrations. < = below detection limit. n.a. = not analyzed.

Table 2 Representative electron microprobe analyses for pyrrhotite, pentlandite, and chalcopyrite from Tejadillas prospect, Cortegana Igneous Complex

Sulfide mineral	Po	Po	Po	Pn	Pn	Pn	Ccp	Ccp	Ccp
wt. %									
Fe	61.51	61.55	61.13	28.46	32.26	32.47	30.74	31.04	30.75
Ni	0.27	0.20	0.24	34.00	32.34	31.49	<	<	<
Cu	<	<	<	<	<	<	34.61	34.24	34.22
Co	0.08	0.09	0.07	4.67	2.88	3.37	0.01	0.03	0.06
Pb	0.24	0.23	0.28	0.22	0.19	0.17	0.24	0.17	0.23
S	38.31	38.11	38.13	32.82	32.97	32.91	34.82	34.72	34.51
Total	100.41	100.18	99.85	100.17	100.65	100.42	100.43	100.21	99.76
apfu									
Fe	0.921	0.927	0.920	3.947	4.447	4.484	1.009	1.020	1.016
Ni	0.004	0.003	0.003	4.487	4.242	4.138			
Cu							0.998	0.989	0.994
Co	0.001	0.001	0.001	0.614	0.376	0.442	0.000	0.001	0.002
Pb	0.001	0.001	0.001	0.008	0.007	0.006	0.002	0.002	0.002
S	0.999	0.999	1.000	7.927	7.912	7.916	1.989	1.987	1.985
Total	1.926	1.931	1.925	17	17	17	4	4	4

Po = pyrrhotite; Pn = pentlandite; Ccp = chalcopyrite. apfu: atoms per formula unit. Recalculation was based on S + Bi = 1 in pyrrhotite, 17 apfu in pentlandite and 4 apfu in chalcopyrite. < = below detection limit.

Gabbronorite and norite are the most common cumulate rocks in the Tejadillas body. They are texturally similar, consisting of medium-grained orthocumulates composed of variable proportions of cumulus orthopyroxene and clinopyroxene, and intercumulus plagioclase and amphibole (tremolitic hornblende, magnesiohornblende and tschermakiite hornblende), and minor amounts of quartz and phlogopite (Fig. 3c). In these rocks, orthopyroxene (Mg# = 0.77–0.82) is commonly more abundant than clinopyroxene (Mg# = 0.80–0.87), although clinopyroxene becomes locally very abundant giving rise to gabbro *s.s.* Mg# values of clinopyroxene in gabbro *s.s.* (Mg# = 0.84–0.86) overlap with those measured in gabbronorites. Clinopyroxene-rich rocks are more altered than orthopyroxene-rich rocks, so clinopyroxene occurs partially to totally altered to actinolite and chlorite, and plagioclase is replaced by sericite and chlorite. In the most leucocratic rocks, plagioclase occurs both as intercumulus grains to pyroxene and fractionating cumulus phases. In both cases, plagioclase commonly exhibits normal zoning with Ca-rich cores ($An_{75–89}$) surrounded by Ca-poor rims ($An_{40–60}$). Poikilitic textures are also common, consisting of pyroxene enclosed by plagioclase or amphibole.

Quartz-diorite is a coarse- to medium-grained leucocratic rock composed mainly of plagioclase ($An_{36–41}$) and quartz with minor amphibole (tremolitic hornblende), biotite and orthopyroxene (Mg# = 0.78–0.76). It has granular texture characterized by interlocking of randomly oriented, idiomorphic to subidiomorphic plagioclases cemented by interstitial quartz (Fig. 3d). The boundaries between quartz-diorite and gabbronorite-norite are sharp, characterized by a ~2-cm wide mixing band with high concentration of pyroxene or amphibole in the quartz-diorite.

The sulfide mineralization in the Tejadillas prospect mostly occurs in harzburgite and gabbronorite-norite, being absent in the most leucocratic rock-types. The ore minerals occur disseminated, representing commonly less than 5 volume % of the rock. They occur as rounded sulfide droplets within silicates (Fig. 3e, f) and, more frequently, as small aggregates located interstitially to silicate framework (Fig. 3g, h). Locally, ore minerals represent up to 30 volume % of the rock (semi-massive ore). Ore minerals consist of pyrrhotite (usually more than 80 volume % of the total sulfides in a given thin section), pentlandite and chalcopyrite. Pentlandite is more abundant than chalcopyrite, and magnetite and pyrite occur as minor phases, the latter locally replaced by pyrrhotite. Results of electron microprobe analyses (Table 2) show that pyrrhotite contains from 61.13 to 61.86 wt % Fe, less than 0.30 wt % Ni and trace amounts of Co (0.06–0.1 wt. %). Pentlandite has from 31.20 to 34.00 wt % Ni, from 28.40 to 32.50 wt % Fe and relatively high Co contents (2.56–4.67 wt. %). Chalcopyrite presents almost stoichiometric compositions, with only trace amounts of Co (0.01–0.07 wt. %).

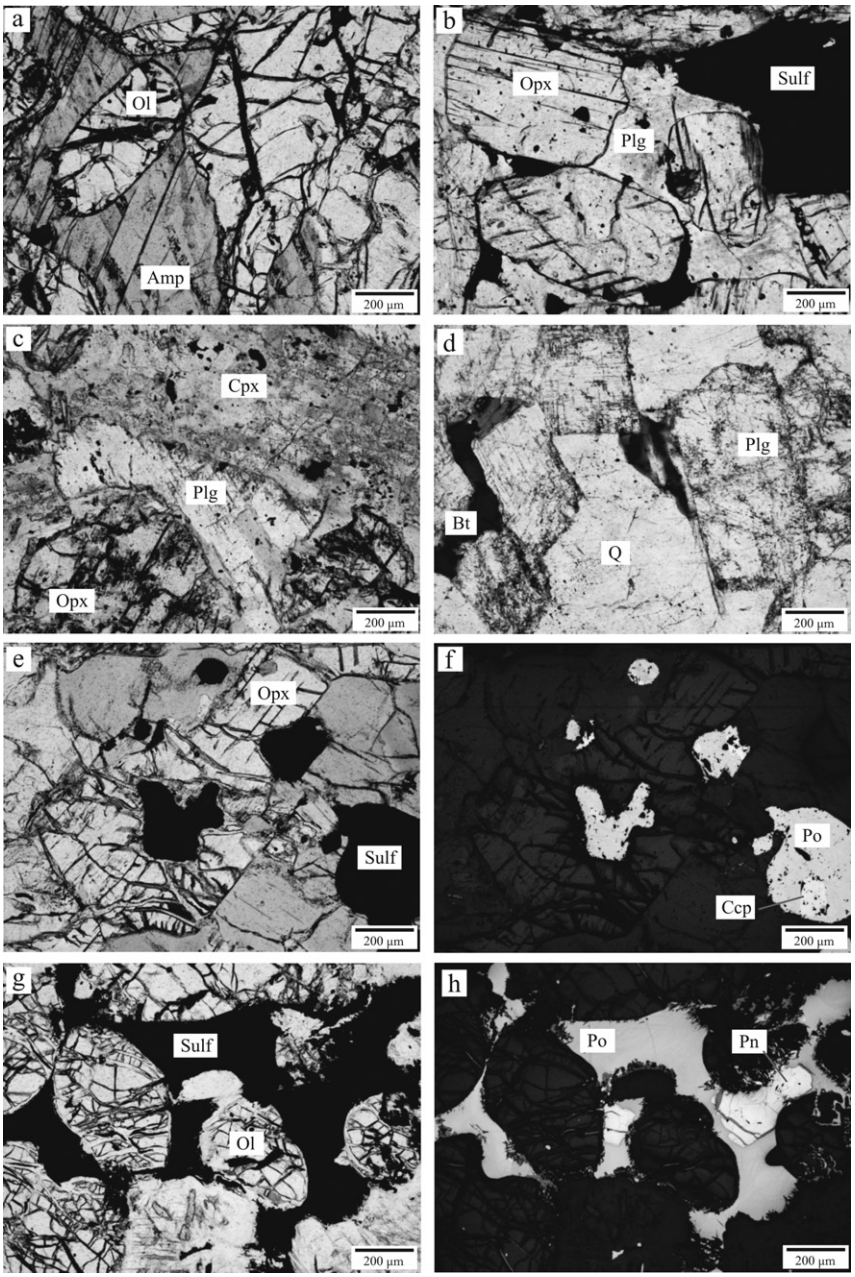

Fig. 3 Photomicrographs under optical microscope of igneous rocks and ore minerals from the Tejadillas prospect of Cortegana Igneous Complex. (a) Olivine (Ol) within poikilitic amphibole (Amp) in hornblende-bearing harzburgite. (b) Cumulus orthopyroxene (Opx) and intercumulus plagioclase (Plg) in norite. Observe the presence of interstitially-located base-metal sulfides (Sulf). (c) Typical textures of clinopyroxene (Cpx), orthopyroxene and plagioclase in gabbronorite. Note that clinopyroxene is patchily replaced by amphibole and contains fine-grained sulfides. (d) Euhedral plagioclase along with interstitial quartz (Q) and biotite (Bt) in quartz-diorite. (e-f) Sulfide droplets composed by pyrrhotite (Po) and minor chalcopyrite (Ccp) within orthopyroxene and amphibole in gabbronorite, under transmitted (e) and reflected (f) light. (g-h) Disseminated sulfides composed of pyrrhotite and minor pentlandite (Pn) located interstitially to olivine in hornblende-bearing harzburgite under transmitted (g) and reflected (h) light.

5. Whole rock geochemistry

In order to describe and compare samples with variable sulfide contents and different alteration grades, the whole rock raw concentrations of the major and trace lithophile elements have been normalized on a sulfide-free basis and to 100% anhydrous silicate composition by correcting for loss-on-ignition (LOI) (the procedure is not shown in this paper, but available on request to the corresponding author). The raw data of whole-rock compositions of major, trace and metal elements are listed in Table 3.

5.1 Major elements

Rocks from the Tejadillas prospect exhibit large compositional variations in agreement with the wide range of modal mineralogy. MgO contents range from 12.30

Table 3 Whole rock major, trace and metal element compositions of igneous rocks from Tejadillas prospect, Cortegana Igneous Complex

Sample No.	17–37	17–73	5–215	5–224	5–93	17–57	17–87	5–81	5–107	5–109	5-167A	5-167B	17–84	17–87	17–92	5–87	5–101	5–173	5–197	5–78	17–61
Rock type	Hz	Hz	Hz	Hz	Ol Gn	GN	GN	GN	GN	GN	GN	GN	N	N	N	N	N	N	Q-d	SM	SM
wt. %																					
SiO_2	47.05	43.46	40.94	38.22	46.67	51.55	49.57	46.73	47.47	49.33	50.2	50.71	46.91	49.53	48.36	47.95	46.88	47.66	57.24	15.32	38.52
TiO_2	0.15	0.17	0.32	0.18	0.46	0.29	0.17	0.36	0.75	0.64	0.45	0.4	0.19	0.31	0.22	0.35	0.64	0.23	0.5	0.08	0.33
Al_2O_3	10.22	7.02	4.95	3.09	9.91	4.62	16.65	3.94	5.76	5.68	5.01	4.43	4.34	5.37	6.61	4.45	5.25	6.15	5.95	2.9	7.61
MgO	19.87	23.94	27.66	29.9	16.8	20.8	12.92	18.42	18.17	19.16	13.58	17.25	21.03	20.65	20.15	20.18	20.14	19.53	14.65	7.11	9.38
Fe_2O_3	11.84	14.31	14.79	16.1	12.27	12.64	7.69	16.7	14.3	12.72	8.91	11.51	18.77	14.43	16.35	17.33	17.49	17.22	13.1	56.72	24.06
MnO	0.169	0.182	0.147	0.13	0.23	0.228	0.131	0.286	0.25	0.258	0.189	0.229	0.228	0.2	0.207	0.284	0.305	0.193	0.166	0.068	0.134
CaO	6.55	6.71	3.33	1.72	9.88	5.98	10.18	8.25	9.15	8.68	17.28	12.01	3.6	5.54	4.58	4.77	3.57	3.99	2.23	2.45	12.56
Na_2O	0.86	0.49	0.53	0.29	1	0.56	1.17	0.62	1.11	1.01	0.96	0.7	0.65	0.66	0.87	0.82	0.9	0.79	0.77	0.65	1.01
K_2O	0.56	0.14	0.72	0.57	0.56	0.37	0.33	0.38	0.36	0.42	0.36	0.37	0.25	0.26	0.27	0.45	0.7	0.32	1.86	0.48	0.52
P_2O_5	0.026	0.021	0.015	0.011	0.035	0.019	0.016	0.025	0.022	0.026	0.024	0.011	0.017	0.023	0.021	0.031	0.03	0.021	0.037	0.017	0.015
S	0.621	1.510	1.603	2.002	1.852	1.497	0.701	3.520	2.578	1.810	1.504	1.641	3.932	2.331	3.227	3.290	3.391	3.694	2.411	17.565	8.257
LOI	2.93	2.89	5.84	7.83	1.36	2.49	1.23	2.38	1.82	1.31	1.58	1.91	1.71	1.64	1.71	2.08	2.72	2.67	2.53	10.15	4.5
Total	100.85	100.84	100.85	100.04	101.03	101.04	100.76	101.61	101.74	101.04	100.05	101.17	101.63	100.94	102.58	101.99	102.02	102.47	101.44	113.51	106.90
ppm																					
Cr	304	736	902	932	504	870	410	684	739	908	817	692	794	782	781	903	839	812	592	125	459
Rb	16.5	2.7	21.9	17.5	15.3	8.9	9.3	12.5	7.6	10.1	10.0	10.4	7.9	7.0	8.0	13.2	21.8	9.2	69.0	16.7	15.3
Ba	63.1	22.9	95.9	66.1	102.8	49.3	46.9	127.3	68.4	73.2	52.7	59.8	34.1	36.8	38.9	71.3	123.4	42.8	208	67.5	79.5
Th	1.77	0.35	0.91	0.58	0.52	0.85	0.35	0.44	0.57	0.59	0.72	0.48	0.62	0.76	0.34	0.53	0.75	0.51	4.83	0.24	0.37
U	0.3	0.13	0.66	0.38	0.39	0.56	0.15	0.3	0.32	0.29	0.67	0.25	0.26	0.37	0.16	0.39	0.47	0.26	3.3	0.1	0.18
Nb	14.86	5.86	3.03	2.44	2.55	7.43	2.89	2.96	3.25	2.92	2.25	2.38	3.87	3.25	3	2.68	3.03	2.05	5.45	1.62	4.7
La	2.25	1.26	4.1	3.04	3.54	3.2	1.63	3.34	3.5	3.95	4.86	3.65	1.73	2.09	1.65	2.76	3.53	2.3	6.33	1.56	3.1
Ce	4.57	2.83	9.3	7.8	8.61	8.82	3.44	8.04	9.72	10.56	13.47	10.53	3.59	4.94	3.49	5.87	7.77	4.49	14.18	3.57	9.16
Pb	7				2	3		4													
Pr	0.53	0.37	1.09	0.97	1.15	1.17	0.41	1.02	1.43	1.53	1.90	1.52	0.38	0.64	0.44	0.72	0.97	0.52	1.64	0.45	1.38
Sr	146	112	28	13	132	39	263	61	61	68	83	60	52	71	95	59	56	73	32	27	106
Nd	2.08	1.7	4.3	4.04	5.57	4.98	1.77	4.46	7.35	7.44	8.94	7.21	1.66	2.84	1.99	3.31	4.37	2.18	6.82	1.86	6.42
Sm	0.47	0.47	1.02	0.89	1.49	1.1	0.47	1.06	2.01	1.84	2.55	2	0.41	0.7	0.48	0.8	1.2	0.52	1.65	0.38	1.72
Zr	27.6	13.6	21.9	21.5	23.9	27.6	11.2	35.5	31.7	29.7	33.5	35.6	13.7	26.5	17.2	23.8	24.8	19.3	39.8	6.1	20.8
Hf	0.71	0.42	0.66	0.64	0.85	0.87	0.33	1.03	1.23	1.11	1.2	1.14	0.4	0.75	0.49	0.76	0.82	0.59	1.47	0.15	0.73
Eu	0.19	0.2	0.26	0.16	0.46	0.25	0.25	0.25	0.51	0.49	0.5	0.39	0.14	0.19	0.18	0.21	0.29	0.19	0.12	0.09	0.36
Gd	0.52	0.55	1.08	0.98	1.83	1.33	0.52	1.27	2.49	2.24	2.98	2.32	0.5	0.94	0.64	0.99	1.48	0.69	2.01	0.46	2
Tb	0.095	0.09	0.186	0.136	0.27	0.217	0.092	0.209	0.398	0.349	0.472	0.38	0.085	0.16	0.09	0.166	0.233	0.115	0.349	0.082	0.316
Dy	0.61	0.63	1.17	0.93	1.83	1.42	0.6	1.39	2.65	2.4	3.27	2.7	0.6	1.03	0.64	1.1	1.56	0.82	2.42	0.48	2.26
Ho	0.12	0.13	0.25	0.2	0.36	0.3	0.12	0.3	0.53	0.49	0.64	0.5	0.13	0.22	0.14	0.24	0.32	0.18	0.55	0.1	0.43
Y	2.98	3.23	5.67	4.82	8.92	7.25	2.93	6.92	12.21	12.35	15.98	13.23	3.1	5.38	3.63	5.84	7.69	4.47	14.19	2.57	9.82
Er	0.42	0.4	0.66	0.57	1.05	0.85	0.38	0.88	1.63	1.35	1.96	1.57	0.44	0.68	0.48	0.67	0.98	0.59	1.67	0.3	1.24
Tm	0.06	0.05	0.09	0.08	0.14	0.13	0.05	0.12	0.21	0.2	0.26	0.23	0.07	0.1	0.08	0.1	0.13	0.09	0.25	0.05	0.17
Yb	0.44	0.41	0.64	0.58	0.99	0.97	0.45	0.95	1.45	1.35	1.74	1.57	0.52	0.71	0.53	0.77	0.91	0.71	1.83	0.35	1.14
Lu	0.072	0.059	0.096	0.083	0.145	0.145	0.067	0.133	0.215	0.203	0.265	0.229	0.091	0.114	0.094	0.119	0.158	0.116	0.294	0.05	0.16
ppm																					
Se	5	7	6	5	7	6	5	11	9	7	9	8	11	7	9	10	9	7	7	13	19
Te	18.1	0.9	0.1	0.1	0.2	10.8	0.3	0.8	0.1	0.1	0.2	0.1	0.5	0.3	0.3	0.6	0.2	0.1	0.2	1.3	1.6
Sb	0.69	0.45	0.17	0.14	0.20	0.58	0.55	0.19	0.22	0.20	0.29	0.27	0.55	0.56	0.58	0.20	0.19	0.18	0.40	0.19	0.58
As	3	3	3	6	2	4	2	2	2	1	3	3	5	3	6	9	6	2	11	12	2
Bi	0.08	0.06	0.08	0.10	0.08	0.10	0.04	0.12	0.06	0.05	0.08	0.08	0.18	0.09	0.10	0.13	0.14	0.12	0.12	0.24	0.34
Ni	873	1118	1488	1574	1324	1366	494	1338	2279	1776	1073	1034	2813	1668	2758	2835	2824	3056	2058	5780	5486
Cu	307	486	545	572	550	542	271	861	776	568	444	484	2783	858	1198	917	679	1125	770	2812	496
Co	99.9	160.0	179.8	215.7	134.2	131.3	66.6	192.7	182.2	142.9	96.0	110.6	262.9	183.3	238.6	243.8	184.3	263.9	168.8	914.4	542.7
Ag	0.7	0.5	0.3	0.2	0.3	0.4	0.4	0.3	0.3	0.3	0.3	0.2	0.6	0.5	0.4	0.3	0.2	0.4	2.4	0.5	0.7
ppb																					
Au	6	11	7	7	10	11	5	11	9	7	5	6	19	11	14	12	12	18	6	16	10
Os																					
Ir																					2
Ru		2				2	3	2	2								3	4	2	2	6
Rh	1	2				3	3	1	2			1	2		1	1	2	3	2	2	6
Pt	7	16	4	8	7	32	25	13	15	6	12	11	18	9	11	17	10	32	19	177	5
Pd	11	18	10	9	15	43	15	19	22	12	18	17	19	12	18	25	24	42	27	43	51

Hz: hornblende-bearing harzburgite; Ol Gn: olivine-bearing gabbronorite; Gn: gabbronorite; N: norite; Q-d: quartz-diorite; SM: semi-massive sulfides-bearing rocks.

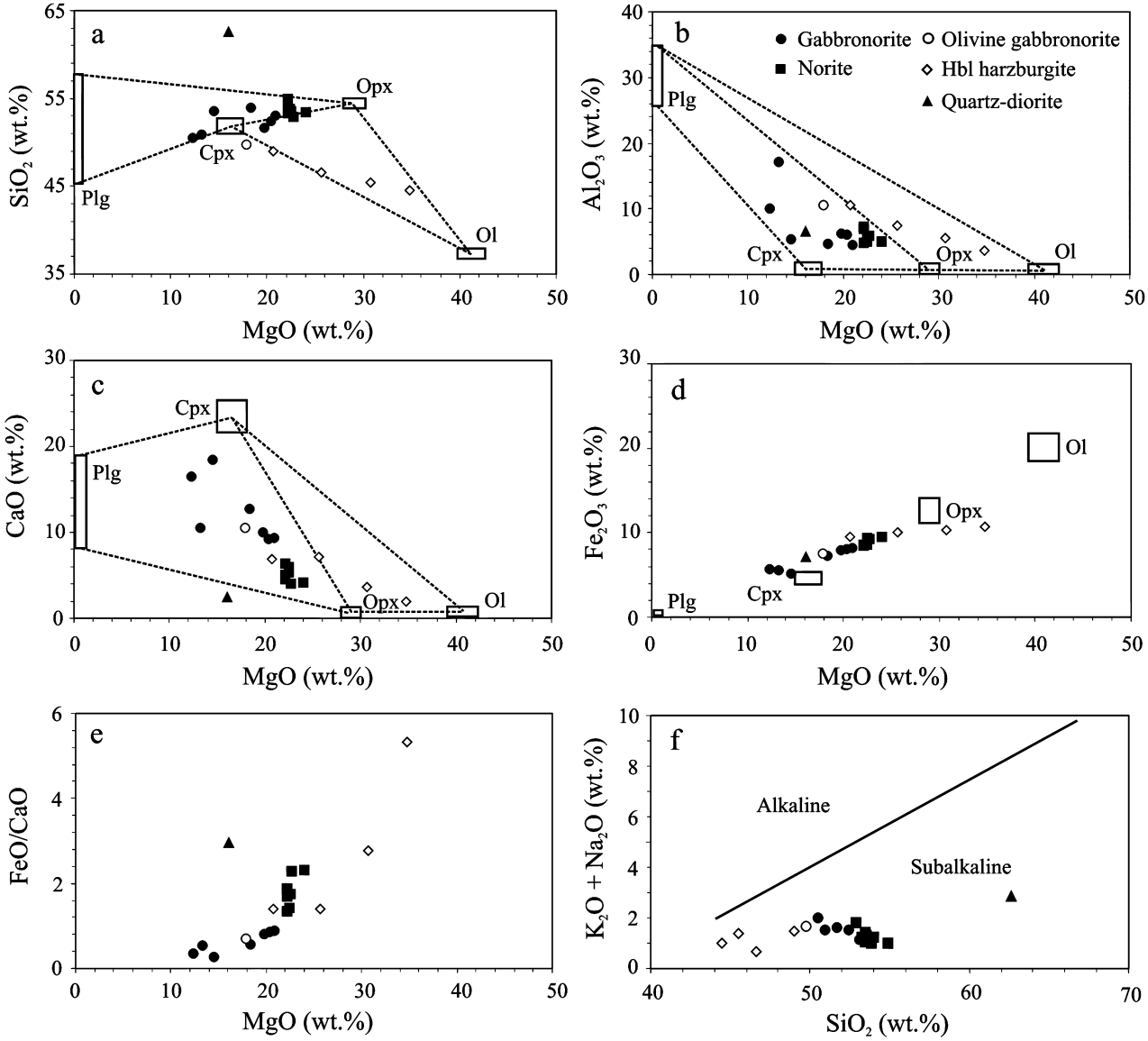

Fig. 4 Binary variation diagrams of SiO_2 (a), Al_2O_3 (b), CaO (c), Fe_2O_3 (d) and FeO/CaO (e) versus MgO. (f) Binary diagram $Na_2O + K_2O$ versus SiO_2 showing the alkaline and subalkaline fields as divided from McDonald and Katsura (1964). Raw data was recalculated to 100 wt. % oxides free of volatiles, water and sulfides. Ol, olivine; Plg, plagioclase; Opx, orthopyroxene; Cpx, clinopyroxene.

to 34.79 wt % and SiO_2 from 44.47 to 62.63 wt %. Mg# values, defined as atomic Mg/(Mg + Fe) ratio, are quite constant, ranging from 0.75 to 0.83. The highest Mg# values correspond to hornblende-bearing harzburgite (Mg# 0.83) in agreement with the high abundance of cumulus olivine. Al_2O_3 contents are relatively low (from 3.60 to 10.64 wt. %), except for a plagioclase-rich gabbronorite sample which contains 17.11 wt % Al_2O_3. All samples are relatively poor in TiO_2 (< 0.82 wt %), MnO (<0.35 wt %) and alkalis (Na_2O+K_2O < 2.88 wt %). Two groups of samples are distinguished in the SiO_2, Al_2O_3, CaO and Fe_2O_3 against MgO binary diagrams (Fig. 4a–d): those plotted between the compositions of olivine, orthopyroxene and clinopyroxene (mostly peridotites), and those represented within the field formed by the compositions of orthopyroxene, clinopyroxene and plagioclase (olivine-bearing gabbronorite, gabbronorite and norite). These diagrams

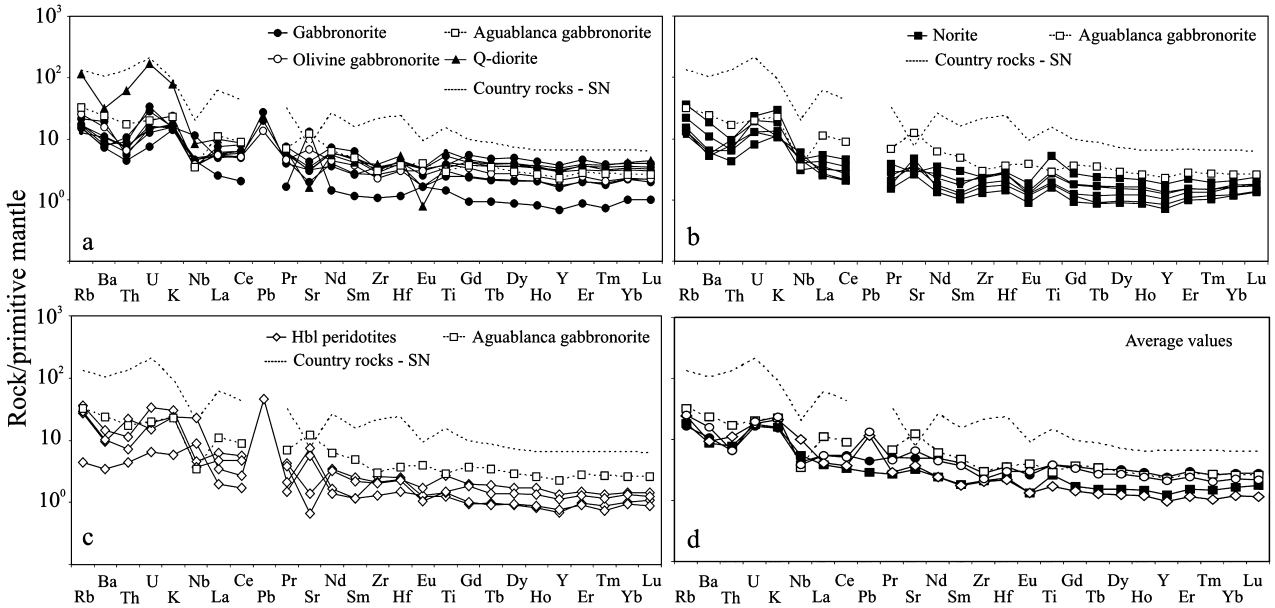

Fig. 5 Primitive mantle-normalized, incompatible trace element patterns for Tejadillas rock samples. (a) Gabbronorite, olivine-bearing gabbronorite and quartz-diorite. (b) Norites. (c) Hornblende-bearing harzburgite. (d) Average value of each rock-type. Normalization factors are from McDonough and Sun (1995). Average composition of the Aguablanca gabbronorite from Piña *et al*. (2006) and that of the country rocks from the Serie Negra Formation from Pereira *et al*. (2006) are shown for comparison.

indicate that peridotite compositions are mainly controlled by the abundance of olivine and pyroxenes, whereas those of gabbronorite and norite are controlled by the modal abundance of pyroxenes and plagioclase. In gabbronorite and norite, pyroxene fractionation was likely to have been more important than that of plagioclase due to the excellent positive correlation between Fe_2O_3 and MgO (Fig. 4d) and the poor correlation between Al_2O_3 and MgO (Fig. 4b). The trend of increasing plagioclase crystallization with decreasing pyroxenes and olivine fractionation from the ultramafic to mafic rocks is well marked by the decrease of FeO/CaO ratio with decreasing MgO (Fig. 4e). On the K_2O + Na_2O versus SiO_2 diagram, all the samples plot in the subalkaline area (Fig. 4f).

5.2 Trace elements

Whole-rock concentrations of trace elements are given in Table 3 and primitive mantle-normalized incompatible element patterns are shown in Figure 5. All patterns are quite similar with the exception of the quartz-diorite sample that has a distinct profile. Samples are characterized by slight enrichment in large ion lithophile elements (LILE), Rb, Ba, Th, U, and LREE, relative to high field strength elements (HFSE) Nb, Ti, Zr, Hf, and HREE. Samples exhibit both negative and positive Sr anomalies, reflecting variable accumulations of plagioclase. Some gabbronorite samples with cumulus plagioclase have extensive positive Sr and minor Eu anomalies. In general, gabbronorites have higher Sm, Ti, Zr and REE contents than norites, probably due to clinopyroxene fractionation that controls the partition of these elements. The relatively high Rb, Ba, K and U concentrations in peridotites are likely to be due to the presence of hornblende. The patterns of the Tejadillas rocks resemble those of Aguablanca (Fig. 5), however, the Tejadillas rocks show slightly less fractionated patterns. Whereas in Aguablanca $(La/Yb)_{MN}$ and $(Th/Nb)_{MN}$ ratios vary from 3.8 to 8.2 and from 2.8 to 9.1, respectively (Piña *et al*., 2006), in Tejadillas these ratios range from 1.6 to 4.4 and from 0.5 to 2.6, respectively. The quartz-diorite sample has higher Rb, Ba, Th and U contents than the rest of cumulates and its profile resembles to that of the meta-sedimentary country rocks (Fig. 5a).

5.3 Base metals, S and PGE

The sulfide ores have low Ni and Cu contents (<0.6 and 0.3 wt. %, respectively) (Table 3). Sulfur contents are

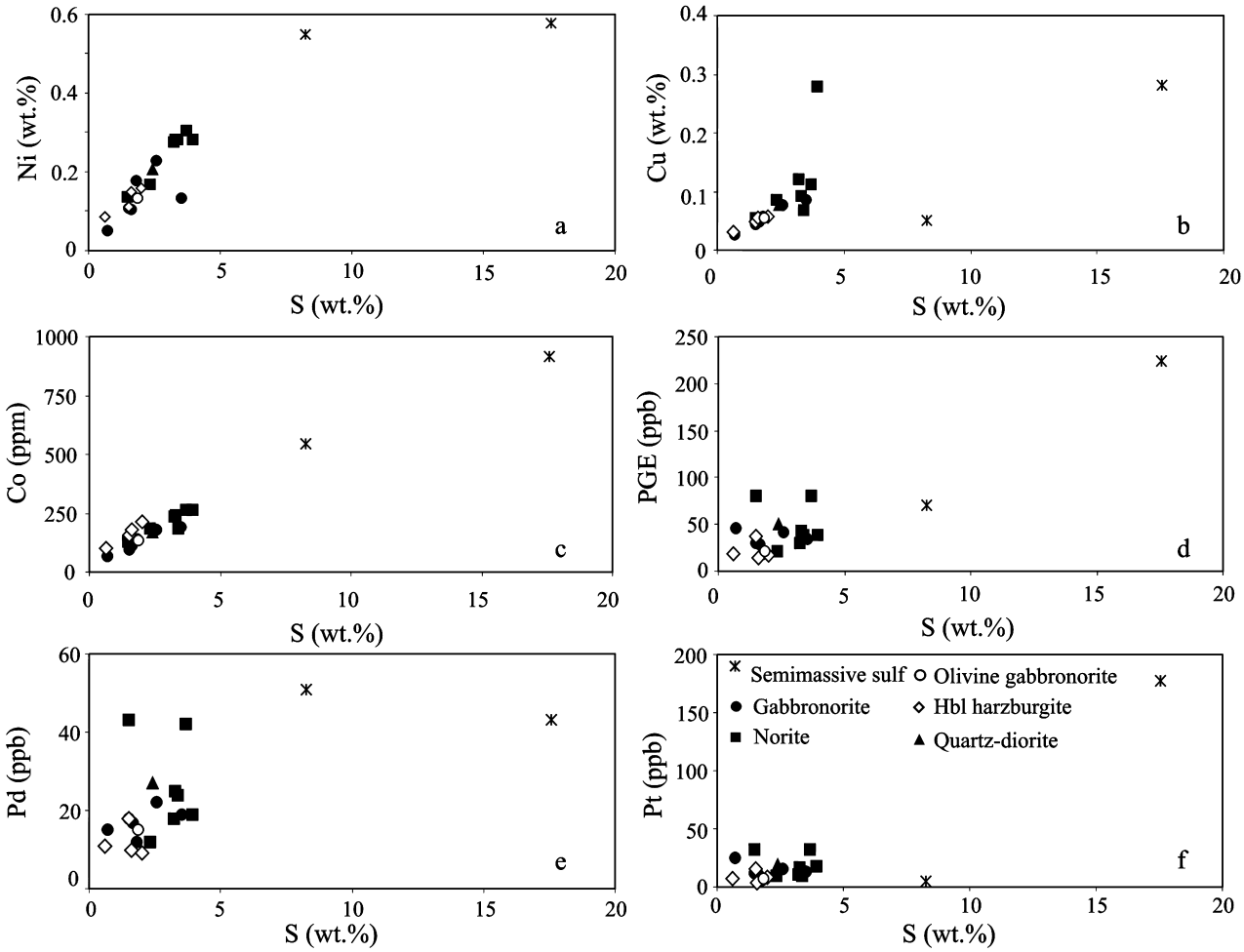

Fig. 6 Binary variation diagrams of Ni (a), Cu (b), Co (c), PGE (d), Pd (e) and Pt (f) versus S of the Tejadillas sulfide ore.

lower than 3.7 wt %, except for the two most sulfide-mineralized samples that host 8.26 and 17.57 wt % S. Nickel and S are well correlated with each other (Fig. 6a), except for the S-richest sample that deviates significantly from the main trend due to its unusually low Ni content. Copper is also well correlated with S (Fig. 6b), but the second most mineralized sample has a lower than expected Cu content by the main trend. Most Ni/Cu ratios range from 1.0 to 3.1, in agreement with the higher proportion of pentlandite relative to chalcopyrite. Selenium concentrations are below 20 ppm and they are positively correlated with S ($\rho = 0.85$, not shown). Se/S ratios range from 74×10^{-6} to 805×10^{-6}; these values are within the empirical range for mantle-derived sulfides (Naldrett, 2004). Cobalt contents range from 67 to 914 ppm and are positively correlated with S (Fig. 6c) and Ni ($\rho = 0.97$ and 0.82, respectively), suggesting that pentlandite is the main carrier of Co. Platinum-group elements show very low concentrations, ranging from 14 to 81 ppb, except for the sulfide-richest sample (17.6 wt. % S) which contains 224 ppb PGE (mainly Pt, 177 ppb) (Fig. 6d). In spite of the fact that the most abundant PGE are Pt and Pd, their contents are generally lower than 32 and 51 ppb, respectively (excluding the above referred Pt-rich sample). Palladium correlates relatively well with S (Fig. 6e) but Pt shows poor correlation (Fig. 6f). Osmium, Ir, Ru and Rh are commonly below or close to the detection limit (<2 ppb). The Tejadillas sulfide ores are poor in Au (<20 ppb) and Ag (<1 ppm). The Au–S correlation is relatively good ($\rho = 0.62$, not shown), except for the S-richest samples that deviate from the main correlation trend due to their unusually low Au contents (10–16 ppb, Table 3).

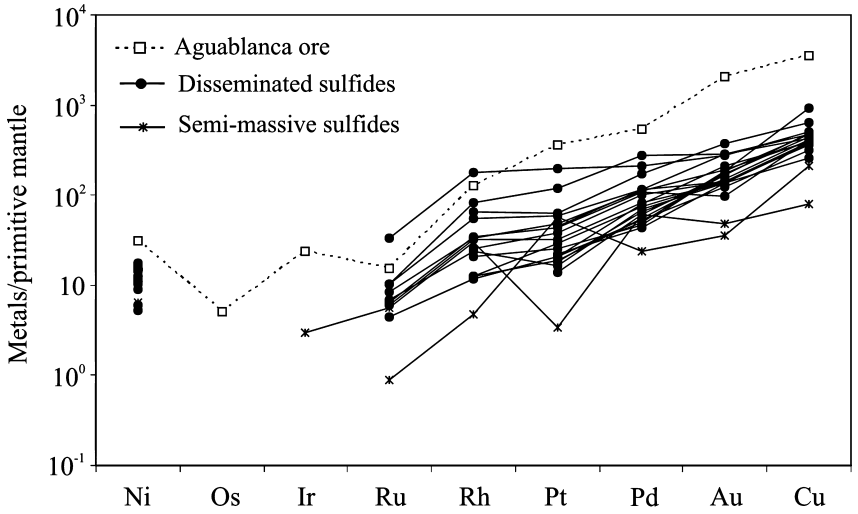

Fig. 7 Mantle-normalized variation diagrams recalculated to 100% sulfide for PGE, Au, Ni and Cu for Tejadillas sulfides. Average composition of the Aguablanca ore from Piña *et al*. (2008) shown for comparison.

Primitive mantle-normalized, PGE, Ni, Cu and Au patters recalculated to 100% sulfides are shown in Figure 7. The normalization to 100% sulfide was carried out to compare metal contents among samples with different sulfide abundance. For the normalization, we followed the method described by Barnes and Lightfoot (2005), and the values below the detection limit were not used. Patterns are broadly similar, with overall positive slopes from Ru to Cu. In all cases, Ni predominates over IPGE (Os, Ir and Ru) and Cu over Pt, Pd, Rh and Au. The two sulfide-rich samples show much more irregular patterns, with most values below those of the less mineralized samples. Patterns of Tejadillas sulfide ores are comparable to those of the Aguablanca sulfide mineralization (Piña *et al*., 2008). However, the Tejadillas sulfide ores are impoverished in all metals relative to those from Aguablanca, suggesting that the former was formed from more depleted silicate magmas in metals than the latter.

6. Discussion

6.1 Nature of the parental magmas

The nature of parental magmas of the Tejadillas rocks of the Cortegana Igneous Complex can be only broadly constrained because such rocks are cumulates and no chilled margin is observed. Olivine composition can provide reliable information on the composition of magmas. Using the most forsteritic olivine composition (Fo_{83} in hornblende peridotite) and a molar Mg-Fe distribution constant ($K_d = (Fe/Mg)^{olivine}/(Fe/Mg)^{magma}$) of 0.30 ± 0.03 (Roeder & Emslie, 1970), the Mg# [atomic Mg/(Mg+Fe) ratio] of the silicate melt is estimated to be 0.59. This value represents a minimum estimation, because Fo content of olivine may be reduced via exchange with trapped liquid as demonstrated by Li *et al*. (2004). However, the Mg# inferred for the Tejadillas magmas is significantly lower than the typical values of mantle-derived primary magmas which range from 0.68 to 0.75 (Wilson, 1989). The value of 0.59 is also lower than the Mg# values of the studied samples (0.78–0.83, Table 3), indicating that such rocks are really cumulates enriched in MgO by olivine and pyroxene accumulation. The inferred Mg# suggests that Tejadillas magmas are likely to be the result of extensive fractionation of melts previous to its final emplacement. In the case of the Aguablanca intrusion, the Mg-richest olivine (Fo_{91}) was found in a peridotite fragment of the mineralized breccia (Piña *et al*., 2006). These fragments were interpreted as belonging to a hidden mafic-ultramafic complex located below the Aguablanca intrusion (Piña *et al*., 2006). The minimum inferred Mg# value for the parental magmas of the peridotite is 0.75, significantly higher than that in Tejadillas and within the range for mantle-derived magmas. Hence, the existence of igneous cumulates below the Aguablanca intrusion formed from more primitive mantle-derived magmas than those of Tejadillas and Aguablanca supports the interpretation of differentiation processes of magmas prior to the emplacement of the Tejadillas and Aguablanca intrusions.

The composition of sulfide ores also provides clues on the composition of silicate melts from which sulfides segregated. Ni/Cu and Pd/Ir ratios are commonly used to discern between sulfides segregated

from ultramafic or mafic magmas (i.e., Keays, 1995; Barnes & Lightfoot, 2005). Sulfides segregated from ultramafic magmas tend to have Ni/Cu and Pd/Ir ratios generally higher than 7 and lower than 10, respectively (e.g., Kambalda, Western Australia, Ni/Cu ~14 and Pd/Ir ~8, Cowden *et al*., 1986). In contrast, mafic magmas commonly produce sulfide ores with Ni/Cu and Pd/Ir ratios lower than 2.5 and higher than 10, respectively (e.g., Noril'sk, Russia, Ni/Cu ~0.5–1.4 and Pd/Ir ~33–160, Naldrett, 2004; Jinchuan, China, Ni/Cu ~0.3–3.3 and Pd/Ir commonly >15, Su *et al*., 2008; Karatongke, China, Ni/Cu ~0.25–2.5 and Pd/Ir ~4–253, Song & Li, 2009). In the sulfide ores from Tejadillas and Aguablanca, both ratios indicate basaltic linkage of the silicate melts rather than ultramafic. Ni/Cu ratios in sulfide-mineralized Tejadillas rocks usually range from 1.0 to 4.2 with an average value of 2.5, whereas the disseminated sulfides in Aguablanca (considered formed from unfractionated sulfide melt) have Ni/Cu ratios ranging from 0.28 to 1.29 (Piña *et al*., 2008). In Aguablanca, Pd/Ir ratios are variable but commonly higher than 22 (Piña *et al*., 2008). In contrast, at Tejadillas, Ir contents are always below the detection limit (2 ppb), so Pd/Ir ratios are not very confident. However, using the detection limit as the maximum Ir value, Pd/Ir ratios range between 4.5 and 25.5 (average, 11.2). Although these values are close to 10, the calculated Pd/Ir ratios actually represent minimum values.

6.2 Role of crustal contamination in the genesis of sulfide ores

Crustal contamination of silicate magmas by assimilation of external sulfur from sulfide-bearing country rocks is a genetic process common to many nickel sulfide deposits (e.g., Noril'sk, Voisey's Bay, Duluth) (Naldrett, 2004, and references therein). Indeed, the incorporation of significant amounts of crust-derived sulfur can lead to sulfide over-saturation in the silicate melt and subsequent segregation of sulfide melts which scavenge Ni, Cu, Co, Au, PGE and other chalcophile elements. The role of this process has been well recognized in the Aguablanca orebody where sulfur over-saturation was caused by assimilation of S-rich black shale from the Late Neoproterozoic Serie Negra Formation, as indicated by the sulfur isotope compositions for pyrrhotite, pentlandite and chalcopyrite ($\delta^{34}S$ = +7.4‰, Casquet *et al*., 2001). Assimilation involved partial melting of the black shale and released of sulfur to the silicate melt. The Serie Negra Formation is the representative formation of the Ossa–Morena Zone, reaching up to 15–25 km depth, and composed by different graphite- and pyrite-bearing rock-types including metacherts, quartz phyllilites, mica schist, metagreywackes and paragneises (Pous *et al*., 2004; Pereira *et al*., 2006). Sulfur content in these rocks is variable but reaches up to 3000 ppm (Piña, 2006).

The role of the crustal contamination in the genesis of the Tejadillas sulfides is much less evident. Close to the boundary of the intrusion with the country rocks, there is a 5 to 10 meter-wide zone characterized by high concentration of rounded enclaves of host rocks in the gabbro (currently hornfels). The abundance of xenoliths gives to the rock an orbicular texture, with the enclaves exhibiting sharp contacts with the igneous cumulates. These textures appear to indicate poor digestion of the xenoliths by the magmas and thus incomplete assimilation processes. Furthermore, the number of xenoliths decreases from the boundaries toward the central parts of the intrusion, suggesting that interaction between magma and host crustal rocks was very heterogeneous and mostly concentrated in the most external parts of the intrusion. Tornos *et al*. (2006) also suggested a lower degree of contamination in the Cortegana rocks relative to Aguablanca from sulfur isotope data obtained on sulfide disseminations ($\delta^{34}S$ values range from –0.1 to +3.1‰).

Crust-contaminated mafic rocks tend to be enriched in Rb, Ba, Th and LREE relative to Y, Zr, Hf and HREE. Although the primitive mantle-normalized trace element patterns of the Aguablanca and Tejadillas rocks are comparable (Fig. 5), suggesting that they have crystallized from similar primary magmas, the Aguablanca rocks show slightly more fractionated incompatible trace element patterns than those of Tejadillas. Furthermore, the shape of the patterns of the Aguablanca rocks resembles those of the Serie Negra Formation (Fig. 5), suggesting that the crustal component in Aguablanca is higher than in Tejadillas rocks. The extent of crustal contamination in the parental magmas of Aguablanca and Tejadillas igneous rocks can be estimated by using the (Th/Yb) versus (La/Sm) diagram (Fig. 8). These ratios are sensitive indicators of crustal contamination and their representation along with the ratios of possible contaminants is useful to constrain the degree of contamination. As possible contaminants we plotted the average ratios of the Serie Negra Formation (Pereira *et al*., 2006), whereas the composition of the primitive mantle (according to McDonough & Sun, 1995) was used as mantle end member. Figure 8 shows that the Aguablanca rocks plot close to the field of the country

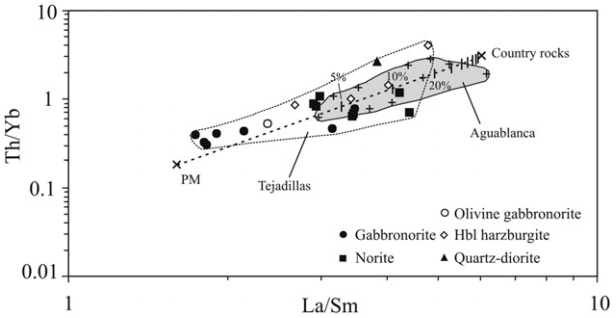

Fig. 8 Plot of (Th/Yb) versus (La/Sm), showing the effect of crustal contamination on trace element ratios for Tejadillas and Aguablanca rocks. The primitive mantle value (PM) is from McDonough and Sun (1995) and the average value for the country rocks of the Serie Negra Formation is from Pereira *et al*. (2006). For the Aguablanca rocks, we use the trace element compositions summarized in Piña *et al*. (2006). Note that the largest crustal component occurs in the Aguablanca rocks (5–30%), whereas the crustal component in the Tejadillas rocks is usually less than 10%.

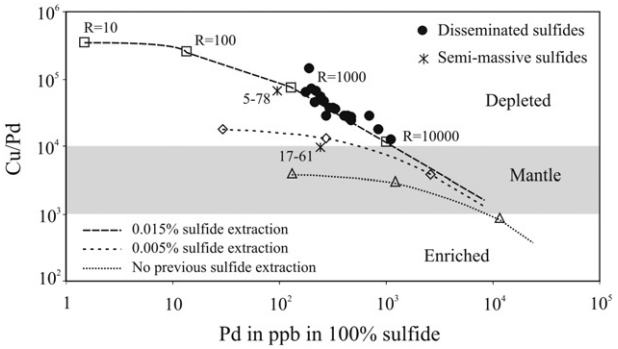

Fig. 9 Plot of the Tejadillas sulfides on the diagram Cu/Pd versus Pd (ppb in 100% sulfides). Note that the composition of the Tejadillas sulfides can be modelled from sulfide melts separated from a PGE-depleted basaltic magma due to 0.015% of previous sulfide extraction at R-factor between 1000 and 10,000.

rocks containing roughly between 5 and 30% of crustal component. In contrast, the Tejadillas samples plot toward the composition of the primitive mantle containing generally less than 5% of sedimentary host rocks. This difference suggests that Aguablanca magmas were more contaminated with country rocks than Tejadillas magmas or, at least, that the contamination process in Aguablanca was much more homogeneous and widespread than in Tejadillas. Thus, whereas in Aguablanca the strong crustal contamination gave rise to the assimilation of abundant external sulfur and, as a consequence, the segregation of high amounts of sulfides, the low degree of contamination documented in Tejadillas inhibited the assimilation of high amounts of sulfur and, as a consequence, promoted the segregation of only minor dissemination of sulfides. Hence, we suggest that the low degree of crustal contamination of the Tejadillas rocks is the key factor to understanding the sparse formation of sulfides.

6.3 Controls on sulfide compositions

The Tejadillas sulfide ores are characterized by their low PGE contents (generally less than 80 ppb, Table 3). Even in samples containing from 1 to 4 wt % S, Os, Ir, Ru and Rh contents are below or very close to the detection limit (2 ppb). Furthermore, preliminary analyses on individual grains of pyrrhotite, pentlandite and chalcopyrite by laser ablation ICP-MS reveal that PGE occur below the detection limit of the technique (6–40 ppb) (Piña *et al*. unpublished data). The low contents in PGE of the Tejadillas sulfide ores are due to the sulfide segregation from PGE-depleted silicate magmas by previous episodes of sulfide segregation and/or PGM removal. Experimental works have shown that PGE are strongly partitioned into the sulfide melts (10^3–10^5, Peach *et al*., 1990), so that early sulfide segregation drastically depletes the residual silicate melt in these metals. Cu/Pd ratios are good indicators of this process. Both Cu and Pd behave as highly incompatible elements in silicate minerals during fractional crystallization of S-undersaturated basaltic melts. Therefore, this kind of fractionation gives rise to constant Cu/Pd ratios roughly reflecting mantle compositions. In contrast, the partition coefficient of Pd between sulfide/silicate melt (~3×10^5) is much higher than that of Cu (~10^3; Peach *et al*., 1990). As a consequence, if a silicate melt reaches S saturation and a sulfide melt is segregated, Pd rapidly incorporates into the sulfide melt resulting in the increase of the Cu/Pd ratio of the residual silicate melt. Sulfides formed later from this residual sulfide melt will have consequently relatively high Cu/Pd ratios. The Tejadillas sulfide ores have Cu/Pd ratios (9700–146,000) higher than those of primitive mantle (Fig. 9), suggesting that sulfides were segregated from a PGE-depleted silicate magma.

It is possible to model the composition of the Tejadillas ores using the following equation:

$$C_i^{sul} = C_i^{sil} * D_i * (R+1)/(R+D_i) \qquad (1)$$

where C_i^{sul} and C_i^{sil} represent the concentrations of the metal i in the sulfide and silicate melt, respectively; D_i is

the sulfide/silicate melt partition coefficient of the metal; and R is the R-factor defined as the mass ratio of silicate melt to sulfide melt (Campbell & Naldrett, 1979). It is assumed that the sulfide/silicate melt partition coefficients are 250 for Cu and 30,000 for Pd, and that Cu and Pd concentrations in the silicate melt are those of typical fertile magnesian basalts with about 12 ppb Pd and 50 ppm Cu (Maier & Barnes, 2010). Using equation (1), the sulfides segregated from the silicate magma would have Cu/Pd ratios lower and Pd values higher than those observed at Tejadillas for various R factors (Fig. 9). However, using the composition of a silicate magma which underwent previous extraction of 0.015% of sulfide melt, the resultant sulfide compositions match quite well with those observed in Tejadillas. According to Rayleigh's Law, the removal of 0.015% of sulfide melt would give rise to a PGE-depleted residual silicate magma containing 48.17 ppm Cu and 0.13 ppb Pd. Further, segregation of a sulfide melt from this PGE-depleted magma under R-factors between 1000 and 10,000 would give rise to the sulfide compositions observed in Tejadillas ores (Fig. 9). The variations of metal contents in some Tejadillas samples can be related with variations in the R-factor. Indeed, sulfides equilibrated at low R-factors tend to have low chalcophile element contents because the interaction of such sulfides with the silicate melt is relatively low. At Tejadillas, the most enriched sulfide samples (5–78 and 17–61, Table 3) contain unusually low Ni and Cu concentrations deviating from the main correlation trend (Fig. 6a, b), and host less PGE than the disseminated samples as well (Fig. 7). The composition of one of the two sulfide-rich samples (5–78) is modelled with the lowest R-factor (~1000, Fig. 9), supporting this interpretation. In contrast, the sample 17–61 is displaced from the model line and cannot be modelled under the same conditions as the rest of samples. Additionally, the low Cu and Pd contents despite the high S concentrations (Table 3) may be due to the presence of high amounts of secondary pyrite replacing pyrrhotite in this sample.

Accordingly, we suggest that the parental magmas of the Tejadillas sulfide ores experienced, at least, two stages of sulfide saturation. The first episode of sulfide segregation took place before the emplacement of the magma, either in staging chambers or en route to its current position, depleting the residual silicate melt in highly chalcophile elements, i.e. PGE. The second stage of sulfide saturation formed the PGE-depleted sulfides currently present in the Tejadillas igneous rocks. This stage is likely to have occurred after the emplacement of the magma in the chamber. The presence of sulfide droplets within early-crystallized silicates (Fig. 3e) and the Ni-depleted nature of olivines and pyroxenes in the most primitive cumulates suggests that sulfide segregation probably took place prior to silicate crystallization. During olivine crystallization, Ni behaves as a compatible element ($D_{Ni}^{olivine/sil}$ ranges from 1.5 to 13, Sugawara & Akaogi, 2003). If an immiscible sulfide melt is present, Ni is preferentially partitioned into the sulfide melt due to its high partition coefficient between sulfide and silicate melt ($D_{Ni}^{sul/sil}$ = 575–836, Peach *et al*., 1990). In this situation, the silicate melt rapidly becomes depleted in Ni as well as olivines formed from this magma (e.g., Thompson & Naldrett, 1984). Therefore, olivine in the ultramafic rocks of Tejadillas prospect likely crystallized coeval with or after sulfide segregation. Sulfide melt was occasionally retained by early-crystallized silicates (Fig. 3e, f) but most was concentrated between silicate grains, giving rise to the disseminated ore (Fig. 3g, h).

6.4 A genetic model for the Tejadillas sulfide ore

The origin of the largest magmatic sulfide deposits is closely related to huge amounts of Ni-rich mafic magmas generated during the activity of mantle plumes (Begg *et al*., 2010). Recently, the existence of a mantle plume below the Ossa–Morena Zone has been inferred from the discovery by deep reflection seismic of a mid-crustal, strongly reflective thick body, called the Iberian Reflective Body (Simancas *et al*., 2003). Although still under debate, this 140 km-long and up to 5 km-thick body seems to represent a large mafic intrusion formed during the activity of a mantle plume in Early Carboniferous (~340–350 Ma). This mantle plume was likely to have been active during a short transtensional tectonic stage intermediate between two main transpressional tectonic regimes associated with an Andean-type subduction zone (Simancas *et al*., 2003, 2006; Carbonell *et al*., 2004). The age both of the Cortegana Igneous Complex and the Aguablanca intrusion (336.2 ± 1.7 and 341 ± 1.5 Ma, respectively, Tornos *et al*., 2006 and Romeo *et al*., 2006), and their geotectonic environment are consistent with the interpretation that these two intrusions are genetically linked with the activity of this voluminous mantle-derived magmatism. Thus, it seems probable that the mantle plume that affected to the Ossa–Morena Zone in Carboniferous was responsible for providing the magmas that formed the Variscan mafic intrusions emplaced

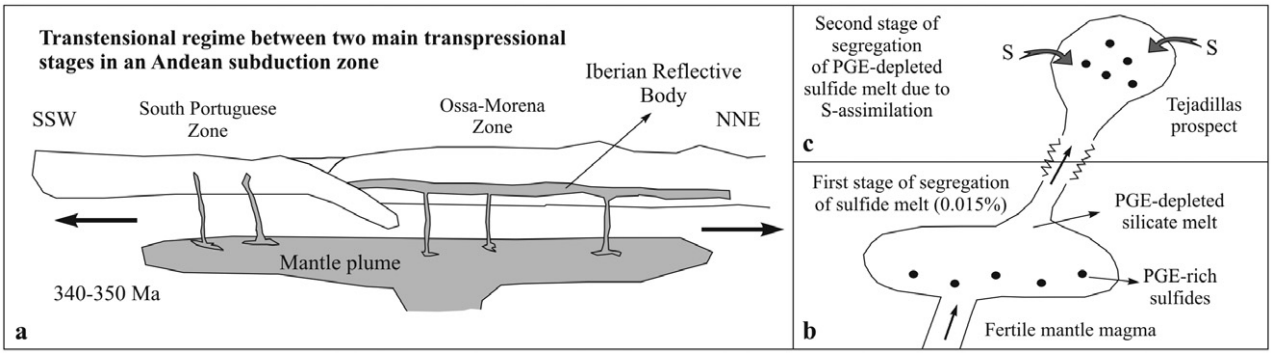

Fig. 10 Conceptual model for the genesis of the Ni–Cu sulfide ore in the Tejadillas prospect. See text for explanation.

across the Ossa–Morena Zone and South Portuguese Zone of the Iberian Massif.

The genetic model for the Tejadillas sulfide ore is schematically illustrated in Figure 10 and outlined below. During the Early Carboniferous (~350–340 Ma), an enormous volume of mantle-derived mafic-ultramafic magmatism was generated as a consequence of the impact of a mantle plume beneath the Ossa–Morena Zone during an extensional stress stage intermediate between two main transpresional tectonic events (Fig. 10a) (Simancas *et al*., 2003, 2006; Carbonell *et al*., 2004). These mantle melts, likely fertile in terms of chalcophile metals, were emplaced and retained at mid-crustal levels forming the so-called Iberian Reflective Body. Magmas migrating from this body at shallower levels of the crust, likely favoured by active faults, eventually reached S saturation and segregated sulfide melts (Fig. 10b). The highly chalcophile elements (e.g., PGE) were rapidly incorporated to this first-stage sulfide melt that may have settled in staging chambers or magma conduits during its ascent throughout the crust. As a result, a PGE-depleted silicate melt was formed and continued its ascent, likely facilitated by the presence of fault-related open conduits under the inferred transtensional, active tectonic regime. Before the emplacement in its current position, the magma evolved from ultramafic to mafic compositions probably by Mg-rich olivine and pyroxene crystallization. This process would explain the more evolved compositions that show the Tejadillas cumulates in comparison with mantle compositions. Once the PGE-depleted and evolved silicate melt reached its current emplacement, it became again sulfide-saturated, likely due to local assimilation of crustal sulfur (Fig. 10c). This event was much less significant than in the case of Aguablanca as shown by the sparse formation of sulfides and relatively few contaminated-nature samples of host igneous rocks. Hence, only small amounts of sulfide melt segregated containing extremely low PGE tenors due to the first-stage sulfide segregation.

7. Conclusions

Geochemical data indicates that the sulfide-bearing igneous rocks of the Tejadillas prospect from the Cortegana Igneous Complex are not very contaminated with the metasedimentary country rocks. The low crustal contamination probably constitutes the key factor to the scarce formation of sulfides in Tejadillas. Whereas in the neighboring Aguablanca, the strong crustal contamination that underwent the magmas involved the assimilation of large amounts of crustal sulfur and subsequent segregation of sulphides. In Tejadillas, the low contamination inhibited the assimilation of significant amounts of sulfur and only small disseminations of sulfides were formed. Furthermore, the Tejadillas sulfide ore became depleted in PGE as a result of previous sulfide segregations before the emplacement and crystallization of the intrusion.

From the point of view of regional exploration, it seems evident that the best targets for Ni–Cu–(PGE) sulfide ores in SW Iberia are those Variscan, mantle-derived mafic-ultramafic intrusions that underwent strong crustal contamination with S-rich metasedimentary country rocks. In addition, in prospecting high-grade metal tenor sulfide ores, it is important to take into account the existence of previous episodes of sulfide extraction at deep levels before the emplacement of the magmas to their final positions, because early sulfide segregations result in PGE-depleted sulfide mineralization such as in Tejadillas.

Acknowledgments

The authors are very grateful to Lundin Mining Corporation for the facilities given for carrying on this research. We would like to thank Professor J. González de Tánago and Mr. A. Larios of the University Complutense of Madrid who kindly assisted in the electron microprobe analyses. We thank Dr. Mei-Fu Zhou for his constructive review and Dr. Yasushi Watanabe for his editorial input which have helped to improve the manuscript. This research was financed by the Spanish research project CGL2007-60266.

References

Barnes, S.-J. and Lightfoot, P. C. (2005) Formation of magmatic nickel sulfide deposits and processes affecting their copper and platinum group element contents. *In* Hedenquist, J. W., Thompson, J. F. H., Goldfarb, R. J. and Richards, J. P. (eds.) One Hundredth Anniversary Volume, Economic Geology, Littleton, CO, 179–213.

Begg, G. C., Hronsky, J. A. M., Arndt, N. T., Griffin, W. L., O'Reilly, S. Y. and Hayward, N. (2010) Lithospheric, cratonic and geodynamic setting of Ni–Cu-PGE sulfide deposits. Econ. Geol., 105, 1057–1070.

Campbell, I. H. and Naldrett, A. J. (1979) The influence of silicate: sulfide ratios on the geochemistry of magmatic sulfides. Econ. Geol., 74, 1503–1505.

Carbonell, R., Simancas, F., Juhlin, C. et al. (2004) Geophysical evidence of a mantle-derived intrusion in SW Iberia. Geophys. Res. Lett., 31, 11601–11604.

Casquet, C., Galindo, C., Tornos, F., Velasco, F. and Canales, A. (2001) The Aguablanca Cu-Ni ore deposit (Extremadura, Spain), a case of synorogenic orthomagmatic mineralization: age and isotope composition of magmas (Sr, Nd) and ore (S). Ore Geol. Rev., 18, 237–250.

Castro, A., Fernández, C., Rosa, J. D., Moreno-Ventas, I. and Rogers, G. (1996) Significance of MORB-derived amphibolites from the Aracena Metamorphic Belts, Southwest Spain. J. Petrol., 37, 235–260.

Castro, A., Fernández, C., El-Hmidi, H. et al. (1999) Age constraints to the relationships between magmatism, metamorphism and tectonism in the Aracena metamorphic belt, southern Spain. Int. J. Earth Sci., 88, 26–37.

Cowden, A., Donaldson, M. J., Naldrett, A. J. and Campbell, I. H. (1986) Platinum-group elements in the komatiite-hosted Fe-Ni–Cu sulfide deposits at Kambalda Western Australia. Econ. Geol., 81, 1226–1235.

Dallmeyer, R. D., Fonseca, P. E., Quesada, C. and Ribeiro, A. (1993)) $^{40}Ar/^{39}Ar$ mineral age constraints for the tectonothermal evolution of a Variscan suture in southwest Iberia. Tectonophysics, 222, 177–194.

De la Rosa, J., Jenner, G. A. and Castro, A. (2002) A study of inherited zircons in granitoid rocks from the South Portuguese and Ossa–Morena Zones, Iberian Massif: support for the exotic origin of the South Portuguese Zone. Tectonophysics, 352, 245–256.

Díaz Azpiroz, M., Castro, A., Fernández, C., López, S., Fernández Caliani, J. C. and Moreno-Ventas, I. (2004) The contact between the Ossa Morena and the South Portuguese zones. Characteristics and significance of the Aracena metamorphic belt, in its central sector between Aroche and Aracena (Huelva). J. Iberian Geol., 30, 23–52.

Fonseca, P., Munha, J., Pedro, J., et al. (1999) Variscan ophiolites and high-pressure metamorphism in southern Iberia. Ofioliti, 24, 259–268.

Keays, R. R. (1995) The role of komatiitic and picritic magmatism and S-saturation in the formation of the ore deposits. Lithos, 34, 1–18.

Li, C. and Naldrett, A. J. (1993) Sulfide capacity of magma: a quantitative model and its application to the formation of sulfide ores at Sudbury, Ontario. Econ. Geol., 88, 1253–1260.

Li, C., Zhanghua, X., Sybrand, A., Ripley, E. M. and Maier, D. M. (2004) Compositional variations of olivine from the Jinchuan Ni–Cu sulfide deposit, western China: implications for ore genesis. Miner. Deposita, 39, 59–172.

Lightfoot, P. C. and Keays, R. R. (2005) Siderophile and chalcophile metal variations in flood basalts from the Siberian Trap, Noril'sk region: implication for the origin of the Ni–Cu-PGE sulfide ores. Econ. Geol., 100, 439–462.

Maier, W. D. and Barnes, S.-J. (2010) The Kabanga Ni sulfide deposit, Tanzania: II. Chalcophile and siderophile element geochemistry. Miner. Deposita, 45, 443–460.

Maier, W. D., Barnes, S.-J., Sarkar, A., Ripley, E., Li, C. and Livesey, T. (2010) The Kabanga Ni sulfide deposit, Tanzania: I. Geology, petrography, silicate rock geochemistry, and sulfur and oxygen isotopes. Miner. Deposita, 45, 419–441.

Martín-Izard, A., Fuertes, M., Cepedal, M., et al. (2006) Reacciones de asimilación de rocas pelíticas en el proceso de formación de las mineralizaciones de Ni–Cu de Argallón, Cortegana y Olivenza (Ossa–Morena). Macla, 6, 297–298 (in Spanish).

McDonald, G. A. and Katsura, J. (1964) Chemical composition of Hawaiian lavas. J. Petrol., 5, 82–133.

McDonough, W. F. and Sun, S.-S. (1995) The composition of the Earth. Chem. Geol., 120, 223–253.

Naldrett, A. J. (2004) Magmatic sulfide deposits: geology, geochemistry and exploration. Springer, Berlin. 727p.

Patiño Douce, A., Castro, A. and El-Biad, M. (1997) Thermal evolution and tectonic implications of pinelcordierite granulites from the Aracena metamorphic belt, Southwest Spain. GAC/MAC Annual Meeting, Ottawa, Abstracts, A-113.

Peach, C. L., Mathez, E. A. and Keays, R. R. (1990) Sulfide melt-silicate melt distribution coefficient for noble metals and other chalcophile elements as deduced from MORB: implications for partial melting. Geochim. Cosmochim. Acta, 54, 3379–3389.

Pereira, M. F., Chichorro, M., Linnemann, U., Eguiluz, L. and Silva, B. (2006) Inherited arc signature in Ediacarn and Early Cambrian basins of the Ossa–Morena Zone (Iberian Massif, Portugal): paleogoegraphic link with European and North African Cadomian correlatives. Precambrian Res., 144, 297–315.

Piña, R. (2006) El yacimiento de Ni–Cu-EGP de Aguablanca (Badajoz): caracterización y modelización metalogenética. Unpublished Ph.D. thesis, University Complutense of Madrid, Spain, 254p (in Spanish).

Piña, R., Lunar, R., Ortega, L., Gervilla, F., Alapieti, T. and Martínez, C. (2006) Petrology and geochemistry of mafic-ultramafic fragments from the Aguablanca (SW Spain) Ni–Cu ore breccia: implications for the genesis of the deposit. Econ. Geol., 101, 865–881.

Piña, R., Gervilla, F., Ortega, L. and Lunar, R. (2008) Mineralogy and geochemistry of platinum-group elements in the Aguablanca Ni–Cu deposit (SW Spain). Miner. Petrol., 92, 259–282.

Piña, R., Lunar, R., Ortega, L. and Gervilla, F. (2009) Estudio preliminar de la mineralización de sulfuros de Ni–Cu asociada a las rocas ígneas de Cortegana (Huelva). Macla, 11, 153–154 (in Spanish).

Piña, R., Romeo, I., Ortega, L., et al. (2010) Origin and emplacement of the Aguablanca magmatic Ni–Cu-(PGE) sulfide deposit, SW Iberia: a multidisciplinary research. Geol. Soc. Am. Bull., 122, 915–925.

Pous, J., Muñoz, G., Heise, W., Melgarejo, J. C. and Quesada, C. (2004) Electromagnetic imaging of Variscan crustal structures in SW Iberia: the role of interconnected graphite. Earth Planet. Sci. Lett., 217, 435–450.

Quesada, C. (1991) Geological constraints on the Paleozoic tectonic evolution of tectonostratigraphic terranes in Iberian Massif. Tectonophysics, 185, 225–245.

Quesada, C., Fonseca, P. E., Munha, J., Oliveira, J. T. and Ribeiro, A. (1994) The Beja-Acebuches Ophiolite (Southern Iberia Variscan fold belt): geological characterization and geodynamic significance. Bol. Geol. Min. España, 105, 3–49.

Ripley, E. M., Park, Y. R., Li, C. and Naldrett, A. J. (1999) Sulfur and oxygen isotopic evidence of country rock contamination in the Voisey's Bay Ni–Cu-Co deposit, Labrador, Canada. Lithos, 47, 53–68.

Roeder, P. L. and Emslie, R. F. (1970) Olivine-liquid equilibrium. Contrib. Mineral Petr., 29, 275–289.

Romeo, I., Lunar, R., Capote, R., et al. (2006) U/Pb age constraints on Variscan Magmatism and Ni–Cu-PGE metallogeny in the Ossa–Morena zone (SW Iberia). J. Geol. Soc. Lond., 163, 837–846.

Seat, Z., Beresford, S. W., Grguric, B. A., Mary Gee, M. A. and Grassineau, N. V. (2009) Reevaluation of the role of external sulfur addition in the genesis of Ni–Cu-PGE deposits: evidence from the Nebo-Babel Ni–Cu-PGE deposit, West Musgrave, Western Australia. Econ. Geol., 104, 521–538.

Simancas, J. F., Carbonell, R., González Lodeiro, F., et al. (2003) Crustal structure of the transpressional Variscan orogen of SW Iberia: SW Iberia deep seismic reflection profile (IBERSEIS). Tectonics, 22, 1962–1974.

Simancas, J. F., Carbonell, R., González Lodeiro, F., et al. (2006) Transpressional collision tectonics and mantle plume dynamics: the Variscides of southwestern Iberia. Mem. Geol. Soc. Lond., 32, 345–354.

Song, X. Y. and Li, X. R. (2009) Geochemistry of the Kalatongke Ni–Cu-(PGE) sulfide deposit, NW China: implications for the formation of magmatic sulfide mineralization in a postcollisional environment. Mineral. Deposita, 44, 303–327.

Su, S., Li, C., Zhou, M.-F., Ripley, E. M. and Qi, L. (2008) Controls on variations of platinum-group element concentrations in the sulfide ores of the Jinchuan Ni–Cu deposit, western China. Mineral. Deposita, 43, 609–622.

Sugawara, T. and Akaogi, M. (2003) Calorimetric measurements of fusion enthalpies for Ni_2SiO_4 and Co_2SiO_4 olivines and application to olivine-liquid partitioning. Geochim. Cosmochim. Acta, 67, 2683–2693.

Thompson, J. F. H. and Naldrett, A. J. (1984) Sulfide-silicate reactions as a guide to Ni–Cu-Co mineralization in central Main. *In* Buchanan, D. L. and Jones, M. J. (eds.) Sulfide deposits in mafic and ultramafic rocks. Institute of Mining and Metallurgical Special Publication, London, 103–113.

Tornos, F., Casquet, C., Galindo, C., Velasco, F. and Canales, A. (2001) A new style of Ni–Cu mineralization related to magmatic breccia pipes in a transpressional magmatic arc, Aguablanca, Spain. Mineral. Deposita, 36, 700–706.

Tornos, F., Galindo, C., Casquet, C., et al. (2006) The Aguablanca Ni-(Cu) sulfide deposit, SW Spain: geologic and geochemical controls and the relationship with a midcrustal layered mafic complex. Mineral. Deposita, 41, 737–769.

Wang, C. Y., Zhou, M. F. and Keays, R. R. (2006) Geochemical constraints on the origin of the Permian Baimazhai mafic-ultramafic intrusion, SW China. Contrib. Mineral. Petrol., 152, 309–321.

Wendlandt, R. F. (1982) Sulphide saturation of basalts and andesite melts at high pressures and temperatures. Am. Mineral., 67, 877–885.

Wilson, M. (1989) Igneous petrogenesis. Chapman and Hall, London, 466p.

Zhang, Z., Mao, J., Chai, F., Yan, S., Chen, B. and Pirajno, F. (2009) Geochemistry of the Permian Kalatongke mafic intrusions, northern Xinjiang, Northwest China: implications for the genesis of magmatic Ni–Cu sulfide deposits. Econ. Geol., 104, 185–203.